Regional Scale Photochemical Model Evaluation of Total Mercury Wet Deposition and Speciated Ambient Mercury

Kirk R. Baker[1]

Jesse O. Bash[2]

[1]U.S. Environmental Protection Agency, Office of Air Quality Planning and Standards

109 TW Alexander Dr., Research Triangle Park, NC 27711 (baker.kirk@epa.gov)

[2]U.S. Environmental Protection Agency, National Exposure Research Laboratory

109 TW Alexander Dr., Research Triangle Park, NC 27711

Abstract

Methylmercury is a known neurotoxin with deleterious health effects on humans and wildlife. Atmospheric deposition is the largest source of mercury loading to most terrestrial and aquatic ecosystems. Regional scale air quality models are needed to quantify mercury deposition resulting from complex emissions sources and physical and chemical processes that govern the fate of mercury in the atmosphere. Total mercury wet deposition estimates from multiple regional photochemical transport models applied at 12 km grid resolution over the continental United States compare well with observations (CAMx fractional error=45%, CMAQ fractional error=33%) despite uncertainties in global mercury emissions inventories and certain chemical transformation pathways. In addition, both CMAQ and CAMx well represent observed diel and seasonal patterns Hg(0) and tend to exaggerate the diel patter of Hg(II) at AMNet monitor locations. The observed fraction of particulate mercury to total oxidized mercury (sum of particulate mercury and Hg(II)) is generally greater in colder months and during overnight hours. The modeling systems tend to capture these patterns but have a systematically lower fraction of particulate mercury to total oxidized mercury, especially in winter months.

Annual total mercury deposition from wet and dry processes is 65% greater in CMAQ compared to CAMx over the entire modeling domain. This is largely due to higher wet deposition in CMAQ and higher dry deposition of Hg(0), which is treated as equilibrium with mercury re-emissions and not modeled in CAMx. A sensitivity using CAMx with Hg(0) dry deposition treated similar to CMAQ resulted in more comparable total mercury deposition estimates. Modeled dry deposition velocities for Hg(II) compare well with the limited experimental data, while Hg(0) dry deposition velocities are lower than published experimental data. A mercury bi-directional flux sensitivity application in CMAQ had the overall effect of reducing total mercury dry deposition and slightly improving ambient Hg(0) performance. The range of the domain

wide total deposition from all model sensitivities was within 25% of the mean but exhibited larger deviations in the individual wet and dry deposition budgets. The contribution of mercury initial conditions and lateral boundary inflow conditions were tracked separately using CAMx source apportionment. Initial contribution to total mercury deposition for the entire model domain falls below 5% after 2 weeks. Boundary contribution to total mercury deposition vary considerably across the continental United States, but ranges between 20 and 99% at MDN monitor locations.

Key words: mercury, air quality modeling, CAMx, CMAQ, AMNet, MDN, deposition

1. INTRODUCTION

Consumption of fish containing elevated levels of methylmercury is the primary vector of human exposure to this toxin and results in deleterious health effects ranging from increased risk of cardiac disease in adults to behavior and neurological development deficits in children (Choi et al., 2009). Methylmercury in wildlife has been linked to a variety of negative health impacts (Scheulhammer et al., 2007;Wolfe et al. 1998). Atmospheric deposition is the primary source of mercury to aquatic and terrestrial ecosystems (Hammerschmidt and Fitzgerald, 2006; Selin, 2009; Selin et al., 2010). Once deposited, inorganic mercury species can be converted to toxic methylmercury through biologically mediated processes (Morel et al., 1998).

Mercury exists in the atmosphere in three forms: gaseous elemental mercury, Hg(0), gaseous oxidized mercury, Hg(II), and particulate bound mercury, Hg(p), which is typically in the fine fraction (<2.5 microns in diameter) (Schroeder and Munthe, 1998). Hg(0) dominates total mercury composition in the atmosphere (greater than 95%) and has a much greater residence time than Hg(II) or Hg(p) due to its near insolubility in water and high vapor pressure which minimize removal through wet and dry deposition processes (Marsik et al., 2007; Schroeder and Munthe, 1998). Hg(II) is soluble, Hg(p) is efficiently scrubbed by precipitation and both Hg(II) and Hg(p) have higher dry deposition velocities than Hg(0) resulting in much shorter residence times. In the atmosphere, mercury cycles between elemental and gaseous oxidized divalent states through oxidation-reduction reactions. These reactions include the gas phase oxidation of Hg(0) to Hg(II) and aqueous phase reactions that can either oxidize Hg(0) to Hg(II) or reduce Hg(II) to Hg(0) (Lindberg et al., 2007; Selin et al., 2007; Si and Ariya, 2008). These competing reactions

can impact mercury's atmospheric residence time by oxidizing Hg(0) to more reactive and readily deposited Hg(II) or reducing Hg(II) to Hg(0).

State and Federal rules have been promulgated that would require emissions reductions of mercury from specific U.S. source sectors (U.S. Environmental Protection Agency, 2007, 2010, 2011; Wisconsin Department of Natural Resources, 2008). It is important to be able to quantify the impacts of past and future regulations to determine optimal and effective mercury emissions control strategies. Regional scale photochemical transport models can be used to characterize the complex source-receptor relationships between emissions and mercury deposition to ecosystems. These models are traditionally evaluated against annual average or episodic total mercury wet deposition measurements (Bullock and Brehme, 2002; Vijayaraghavan et al., 2007). The Atmospheric Mercury Network (AMNet) began making routine sub-hourly measurements of speciated ambient mercury in 2008 and 2009, providing a unique opportunity to assess how well photochemical transport models estimate observed diel and seasonal patterns of ambient speciated mercury: Hg(0), Hg(II), and Hg(p).

Regional scale photochemical models simulate mercury emissions, chemical cycling, and deposition. The Community Multi-scale Air Quality (CMAQ) model version 4.7.1 and the Comprehensive Air Quality Model with Extensions (CAMx) version 5.30 have different dry deposition schemes, gas-phase, and aqueous phase mercury chemistry. Both models are applied with the same emissions, boundary conditions, and meteorology for the entire year of 2005 at 36 and 12 km grid resolution covering the continental United States. Model estimates of total mercury wet deposition and rainfall are directly compared to measurements at monitors in the Mercury Deposition Network (MDN). A qualitative evaluation of both models is made with observations from the Atmospheric Mercury Network (AMNet) monitor network to determine how well seasonal and diel patterns are represented. Additional sensitivity simulations at 36 km grid resolution are done with both CAMx and CMAQ to better bound total wet and

dry deposition estimates. The impact of initial and boundary conditions on annual regional scale mercury modeling simulations is variable and has been shown to dominate contribution to total mercury deposition (Pongprueksa et al., 2008). The CAMx model is also applied with mercury source apportionment to estimate the contribution from initial and boundary conditions to total mercury deposition.

2. METHODS

2.1 Photochemical Model Background

CMAQ simulates the formation and fate of photochemical oxidants, ozone, primary and secondary particulate matter, and air toxics over regional and urban spatial scales for given input sets of meteorological conditions and emissions (Byun and Schere, 2006; Foley et al., 2010). CMAQ is applied with the AERO5 aerosol module, which includes ISORROPIA inorganic chemistry (Nenes et al., 1999) and a secondary organic aerosol module (Carlton et al., 2010). The CMAQ model is applied with sulfur and organic oxidation aqueous phase chemistry (Carlton et al., 2008) and the carbon-bond 2005 (CB05) gas-phase chemistry module (Yarwood, 2005). Mercury oxidation pathways are represented for both the gas and aqueous phases in addition to aqueous phase reduction reactions (Bullock and Brehme, 2002) (Table 1).

CAMx includes numerous science modules that simulate the emission, production, decay, deposition and transport of organic and inorganic gas-phase and particle-phase pollutants in the atmosphere (Baker and Scheff, 2007; Nobel et al., 2001; Russell, 2008). CAMx is applied with ISORROPIA inorganic chemistry (Nenes et al., 1999), a semi-volatile equilibrium scheme to partition condensable organic gases between gas and particle phase (Strader et al., 1999), Regional Acid Deposition Model (RADM) aqueous phase chemistry (Chang et al., 1987), and

CB05 gas-phase chemistry module (Yarwood, 2005). Mercury oxidation pathways are represented for both the gas and aqueous phases in addition to aqueous phase reduction reactions (ENVIRON, 2010) (Table 1).

CAMx and CMAQ have similar aqueous phase oxidation reactions but different reduction reactions; CAMx reduces mercury with the hydroperoxyl radical and CMAQ reduces mercury with dicarboxylic acid (DCA) and photolytic breakdown (Si and Ariya, 2008). Research suggests that the aqueous phase reduction reaction involving hydroperoxyl radical under typical atmospheric conditions is improbable (Gardfeldt and Jonsson, 2003). Gas phase oxidation reactions are similar between models with the exception of the yields from ozone oxidation. Mercury oxidation in the gas phase by ozone yields 50% Hg(p) and 50% Hg(II) in CMAQ (Pal and Ariya, 2004a). Gas phase oxidation of Hg(0) by ozone yields 100% Hg(II) in CAMx (Hall, 1995).

Dry deposition of all mercury species is characterized in CMAQ using the M3DRY deposition scheme (Pleim, 2004). CAMx dry deposition of Hg(II) and Hg(p) is modeled following the Wesely resistance based approach (Wesely, 1989). CAMx assumes that the magnitude of Hg(0) dry deposition is equivalent to emissions from natural sources so dry and wet deposition is assumed to be negligible (ENVIRON, 2010). Thus in CAMx, Hg(0) is only being removed by chemical transformation to Hg(II). Since mercury emissions from natural sources are included in the emission inventory for these simulations, an additional CAMx sensitivity was done for the entire year of 2005 at 36 km grid resolution that includes dry and wet deposition of Hg(0). The reference Henry’s law constant and temperature dependency for Hg(0) and molecular diffusivity

ratios of Hg(0) and Hg(II) are set to be consistent with CMAQ for this model sensitivity (Clever et al., 1985; Massman, 1999). An additional sensitivity using CMAQ v4.7.1 with a bi-directional flux model for Hg(0) is applied for the entire year of 2005 at 36 km grid resolution to further bound the variability in Hg(0) deposition due to model parameterizations (Bash, 2010). This simulation is the same as the base CMAQ simulation except “Land-Direct” and “Ocean-Direct” emissions are omitted from the simulation and the bi-directional flux module is activated. These estimates of recycled mercury emissions are parameterized in the bi-directional flux model and their inclusion in this sensitivity would constitute a double-counting of these emissions.

2.2 Photochemical Model Application and Inputs

Model simulations were run for a domain covering the continental United States (Figure 1). This domain has a parent horizontal grid of 36 km with two finer-scale 12 km grids over portions of the eastern and western U.S. The model extends vertically from the surface to 100 millibars using a terrain following sigma-pressure coordinate system. Air quality conditions at the outer boundary of the 36 km domain were taken from a GEOS-CHEM Hg simulation and vary in time and space (Selin et al., 2007). The 36 km grid was used to establish the incoming air quality concentrations along the boundaries of the 12 km grids. The base CMAQ and CAMx simulations were run for the entire year of 2005 at 36 and 12 km grid resolution. A total of 10 days at the end of 2004 are simulated but not used in the analysis to minimize initial condition influence for the 36 km domain (Pongprueksa et al., 2008). Only 3 days of spin-up are used for the 12 km domains since they are initialized from the 36 km domain.

Dynamic one-way three-hourly lateral boundary and initial species concentrations for the 36 km domain were provided by the three-dimensional global atmospheric chemistry model GEOS-CHEM (standard version 7-04-11). This model was run for 2005 with a grid resolution of 2.0 degree x 2.5 degree (latitude-longitude) and 30 vertical layers up to 100 mb. The GEOS-CHEM simulation used a 2000 based global anthropogenic emissions inventory that includes 1,278 Mg/yr of Hg(0), 720 Mg/yr of Hg(II), and 192 Mg/yr of Hg(p) (Selin et al., 2007).

Particulate matter source apportionment technology (PSAT) implemented in CAMx estimates the contribution from initial conditions, boundary conditions, and specific emissions source groups using reactive tracer (ENVIRON, 2010; Wagstrom et al., 2008). Tracer species are estimated with source apportionment algorithms rather than by the host model routines. Non-linear processes like gas and aqueous phase chemistry are solved for bulk species and then apportioned to the tagged species. CAMx mercury source apportionment is applied to the annual 2005 simulation at 36 km grid resolution to track the contribution of initial and boundary conditions.

The emissions data are based on the U.S. EPA 2005 National Emissions Inventory (http://www.epa.gov/ttn/chief/net/2005inventory.html#inventorydata). This modeling application included mercury emissions from the National Air Toxics Assessment inventory and boiler sector mercury emissions based on an engineering analysis. Emissions are processed to photochemical model inputs with the Sparse Matrix Operator Kernel Emissions (SMOKE) emissions modeling system (Houyoux et al., 2000). Other North American anthropogenic emissions are based on a 2006 Canadian inventory. Global emissions (including portions of Canada and Mexico) are included in the modeling system through boundary condition inflow.

Annual total mercury emissions included in the 36 km modeling domain are shown in Table 2 by source group.

The “Land – Direct” emissions category (Table 2) includes anthropogenic emissions of Hg(0) from sources such as mining operations and geogenic sources including mercury enriched soil. The National Emissions Inventory estimate of this category was reduced from previous inventories by a factor of 10 to match recent published estimates (Gustin et al., 2008). Elemental mercury emissions from oceans are included in the "Ocean - Direct" category and do not account for near surface deposition or oxidation reactions. The land and ocean re-emission categories are net flux emissions approximating Hg(0) re-emission after total mercury deposition has been taken into account (Bullock and Brehme, 2002). These emissions were not included when the dynamic bidirectional air-surface exchange model was employed to avoid double counting (Bash, 2010). Molecular chlorine emissions are estimated as a continuous emission rate over all ocean water surfaces (Bullock and Brehme, 2002). CAMx does not use molecular chlorine emissions, relying instead on time-invariant vertical profiles of ambient chlorine (ENVIRON, 2010).

Annual gridded meteorological input data for 2005 were derived from simulations of the Pennsylvania State University / National Center for Atmospheric Research Mesoscale Model (MM5) version 3.7.4. MM5 is a limited-area, nonhydrostatic, terrain-following system that solves for the full set of physical and thermodynamic equations which govern atmospheric motions (Grell et al., 1994). Key physics options include the Pleim-Xiu boundary layer and land surface schemes (Pleim and Xiu, 1995), Kain-Fritsh 2 cumulus parameterization (Kain, 2004),

Reisner 2 mixed phase moisture scheme (Reisner et al., 1998), RRTM longwave radiation scheme (Mlawer et al., 1997), and Dudhia shortwave radiation scheme (Dudhia, 1989). Three dimensional analysis nudging for temperature and moisture was applied above the boundary layer only. Analysis nudging for the wind field was applied above and below the boundary layer. The MM5 simulations contain 34 vertical layers with an approximately 38 m deep surface layer and a 100 millibar top.

2.3 Network Measurement Data

Weekly total mercury wet deposition observations taken during 2005 at Mercury Deposition Network (NADP; http://nadp.sws.uiuc.edu/MDN/) monitor locations, which operate under the National Atmospheric Deposition Program (Vermette et al., 1995), are quantitatively compared to model estimates. These NADP sites also collect rainfall data which is compared to precipitation estimates from the prognostic meteorological model, which supplies rainfall as an input to the photochemical models. Both photochemical models output hourly wet and dry deposition estimates of Hg(0), Hg(II), and Hg(p) in each grid cell and are summed to weekly totals to match observations. Total mercury deposition is defined as the sum of all wet and dry deposition of Hg(0), Hg(II), and Hg(p).

Ambient Hg(0), Hg(II) and Hg(p) observations at 24 Atmospheric Mercury Network (AMNet; http://nadp.sws.uiuc.edu/amn/) monitors from 2009 were used to qualitatively evaluate modeled ambient concentrations since the network was not in operation during the modeling period of 2005. AMNet monitor locations collect high time resolution measurements of speciated mercury atmospheric concentrations using Tekran ambient air Hg speciation units, models 2537a/1130/1135, with detection limits of 0.01 ng m^{-3}, 1.0 pg m^{-3} and 1.0 pg m^{-3} for Hg(0),

Hg(II), and Hg(p) respectively (Landis et al., 2002) . Measurement data are averaged over each hour to match with hourly model output. Locations of MDN and AMNet sites included in this analysis are shown in Figure 1. Model outputs for total wet deposition and ambient mercury species are compared to observations using correlation coefficient, mean bias, mean error, fractional bias, and fractional error. Model performance is best when the correlation coefficient approaches 1 and the other metrics approach 0 (Baker and Scheff, 2008).

3. RESULTS and DISCUSSION

3.1 Modeled Mercury Deposition

Annual wet and dry deposition totals over the 36 km modeling domain are shown in Table 3 by specie for the base CAMx, base CMAQ, CAMx sensitivity, and CMAQ bi-directional flux sensitivity simulation. Total mercury deposition over the entire modeling domain is higher in the base CMAQ simulation compared to the base CAMx simulation. Much of this difference is attributable to higher dry deposition of Hg(0) and wet deposition of Hg(II) for CMAQ. Total mercury deposition over the continental United States predominantly consists of Hg(II) in CMAQ (71%) and CAMx (98%). In both models Hg(p) contributes minimally to wet and dry deposition. Dry processes account for 79% (259 Mg) of annual total modeled mercury deposition in CAMx and 57% (311 Mg) in CMAQ (see Figure S-1 for spatial representation). These differences in dry deposition are partly attributable to higher estimated ambient concentrations of Hg(0), partly due to Hg(0) not participating in wet or dry deposition removal processes in CAMx.

When CAMx allows Hg(0) to participate in deposition processes, deposition totals are similar to the base CMAQ, although spatial patterns become less similar (Figure 2). The CMAQ bi-directional flux sensitivity results in deposition totals and spatial patterns closer to the base CAMx simulation. The CMAQ simulation using bi-directional flux shows a net emissions flux of Hg(0) over the entire modeling period, largely due to ocean and soil re-emission (re-emissions are in the form of Hg(0)).

The contribution from initial conditions as a percentage of model domain total mercury deposition falls below 5% after 2 weeks for both the summer and winter simulations (Figure S-2). The summer period initial conditions require additional time to be removed compared to the winter period. These contribution estimates suggests a spin-up period of one to two weeks is adequate in reducing influence from initial conditions to total mercury deposition. The boundary contribution to weekly total mercury deposition varies considerably across MDN locations, ranging from a minimum of 20% to a maximum near 99% (50th percentile = 76%; N=4,497). On an annual basis, boundary conditions dominate at monitors closest to the edge of the modeling domain and at monitors in the western U.S. Areas of decreased boundary condition influence tend to coincide with areas of anthropogenic emissions sources.

3.2 Comparison to Wet Deposition Observations

MM5 modeled rainfall over-estimated observations during the warm months and compared well during the colder months (Figure 3). An evaluation of annual CMAQ and CAMx wet deposition estimates at 12 km grid resolution against 88 NADP locations in the United States and Canada

shows that CAMx under estimated wet deposition (fractional bias of -41% and fractional error 45%) and CMAQ had a small over estimation (fractional bias of 15% and fractional error 33%). Total mercury wet deposition performance for both models is consistent with previously published modeling results (Bullock and Brehme, 2002; Vijayaraghavan et al., 2007).

The distribution of observed and modeled total mercury wet deposition is shown in Figure 4 and average performance metrics over all monitors in each 12 km domain are presented in Table 4. CAMx compares well with observations during the colder months, but under-estimates during the warmest months most notably in the southeastern U.S (Figure S-3). CMAQ shows a less pronounced underestimation tendency in the eastern U.S. during the summer months, but over-estimates total mercury wet deposition in the western U.S. Wet deposition was not sensitive with CMAQ bidirectional exchange as previously published (Bash 2010). The deposition sensitivity in CAMx also had a minimal impact on wet deposition results (Figure S-4).

MM5 systematically over-estimated rainfall at MDN monitor locations in the western U.S. and this partially explains CMAQ over-estimated wet deposition (Figure S-5). CAMx does not show a similar relationship between rainfall performance and total wet mercury deposition performance. The relationships between rainfall bias and total mercury wet deposition bias in CAMx and CMAQ suggests that these models respond differently to aloft Hg(II) and Hg(p) and the lateral boundary conditions. The systematic over-estimation of total mercury wet deposition in the western U.S. compared to the eastern U.S. in CMAQ may also be an indication that CMAQ is sensitive to the ambient Hg(II) and Hg(p) mercury inflow from the western boundary in the free troposphere.

3.3 Comparison to Ambient Observations

Since the AMNet network did not began routine measurement of ambient mercury until late 2008, model estimates of ambient speciated mercury are qualitatively compared to AMNet measurements from 2009 on a monthly (Figure 5) and hourly basis (Figures 6). Only the eastern 12 km domain was used in this evaluation due to the sparse sampling of AMNet sites in the western 12 km domain (Figure 1). Even though the observations and model estimates are temporally incommensurate (i.e., large scale meteorological differences between years and changes in emissions), the modeled distributions are higher than observed over all months and for all species. This suggests there may be too much mercury being put into the modeling system in the emissions or boundary conditions. The modeling systems do replicate general seasonal patterns in ambient speciated mercury. Elemental and particle bound mercury concentrations are lowest during the summer months in the ambient measurements and model estimates.

The ambient concentrations of Hg(II) have been increased by 30% to account for possible sampling loss, but both modeling systems still overestimate ambient Hg(II) and CAMx in particular tends to exaggerate the seasonal and diel profile. Mercury halides have been shown to be released from KCl denuders employed at AMNet sites in the presence of ozone resulting in low bias in the measurements (Lyman et al., 2010). Laboratory experiments have shown losses of approximately one third of Hg(II) as $HgCl_2$ and $HgBr_2$ on KCl denuders in the presence of ozone concentrations as low as 50 ppb (Lyman et al., 2010). Potential Hg(II) measurement artifacts are largest during the summer months and during the daytime hours due to elevated

oxidant concentrations, which may partially explain the modeling systems tendency to overestimate Hg(II). The observed and modeled fraction of particulate mercury of total oxidized mercury, the sum of Hg(II) and Hg(p), decreases during the daytime hours and warmer months (Figure 7). However, the observed particulate fraction tends to be higher throughout the year than modeled, particularly during the coldest months when thermodynamics favor the particulate form of oxidized mercury.

The CAMx sensitivity and CMAQ bi-directional flux sensitivity both generally estimated lower ambient Hg(0) which tends to be closer to concentrations typically observed at AMNet monitors. CMAQ bi-directional flux estimates of Hg(0) are further from typical observed values in the coldest months (Figure S-6). The GEOS-Chem boundary condition Hg(0) concentrations are highest from December through March and are likely driving the winter Hg(0) bias in the model observations due to the relatively lower abundance of oxidants in winter. However, the deposition parameters in the bi-directional flux model are a function of temperature and incoming solar radiation and the slight model performance degradation during December through February may be related to biases in the meteorological inputs or the bi-directional parameterizations. Wet deposition changed little because Hg(0) is relatively insoluble and the oxidation of Hg(0) to Hg(II) is relatively slow resulting in negligible changes in total mercury wet deposition (Figure S-4).

3.4 Modeled Dry Deposition Velocities

Experimental studies indicate Hg(0) dry deposition velocities estimated with periods of measured evasion omitted range from 0.1 to 0.4 cm/s and Hg(II) dry deposition velocities range from 0.5 to 6 cm/s (Zhang et al., 2009). Modeled dry deposition velocities for Hg(II) compare well to experimental data: CAMx 1st and 3rd quartile estimates are 0.7 and 3.9 cm/s and CMAQ 1st and 3rd quartile estimates are 0.7 and 4.7 cm/s. Modeled terrestrial dry deposition of Hg(0) in CMAQ is several orders of magnitude lower than experimental estimates with 1st and 3rd quartile estimates of 0.003 and 0.034 cm/s. The base CAMx simulation has no dry deposition estimate of Hg(0) and the sensitivity simulation estimates of 1st and 3rd quartiles 0.004 and 0.007 cm/s are also below experimental estimates. This low bias in deposition velocity may partially explain high bias in model estimates of ambient Hg(0) concentrations. It is important to note that Zhang et al. (2009) only estimated Hg(0) deposition velocities when deposition was being measured and did not consider the bidirectional exchange of Hg(0).

Modeled dry deposition velocities at AMNet monitor locations for Hg(0) and Hg(II) increase in the CAMx sensitivity simulation (Figures S-7 and S-8). CMAQ estimated dry deposition velocities are similar to CAMx for Hg(II) indicating that the differences between CMAQ and CAMx Hg(II) dry deposition are due to higher yields of Hg(II) in CAMx, as shown in Table 1. However, the lack of mercury dry deposition observations makes it impossible to determine whether the results of this sensitivity lead to better estimates of mercury dry deposition, but highlights the similarities and differences of the modeling systems.

4. CONCLUSIONS

Regional photochemical models are needed for a spatially and temporally complete characterization of the complex nature of mercury in the atmosphere and elucidate regional to local scale source-receptor relationships. Atmospheric mercury chemical mechanisms contain considerable uncertainties in the reaction mechanisms and rates, but, despite the uncertainties, current photochemical model mercury wet deposition and ambient estimates compare well with the observed magnitude and seasonal trends. Improvements in mercury chemical mechanisms and observational data are needed to further characterize the local, regional, and global impacts of controllable and geogenic sources of mercury emissions.

Regional modeling of mercury, particularly in coastal areas, may be improved with increased spatial and temporal treatment of molecular chlorine and bromine emissions over oceans. Bromine chemistry and the inclusion of bromine emissions from ocean surfaces should be implemented to better characterize ambient mercury concentrations and deposition to arctic and high latitude marine regions in photochemical models (Holmes et al., 2010). In addition, the CAMx modeling system would benefit from allowing input of molecular chlorine emissions rather than using an internally fixed vertical profile.

Allowing Hg(0) dry deposition in CAMx reduced ambient Hg(0) estimates at AMNet sites generally improving the agreement between modeled and observed ambient concentrations. This change improved agreement with published experimental dry deposition values, but the dry deposition velocity for Hg(0) in CAMx and CMAQ are much lower than published values and need further investigation. A sensitivity including mercury re-emission (bi-directional flux) did

not change wet deposition performance, but generally estimated ambient concentrations of elemental mercury closer to values observed.

Model estimates of wet deposition have been extensively evaluated against observations and the seasonal and annual biases in photochemical transport models have been quantified (Bullock et al., 2009). However, discrepancies exist between model comparisons of wet deposition in complex terrain, the western domain in this study, and in the parameterization and magnitude of dry deposition. CAMx sensitivities that increased the dry deposition loading by 65% had negligible impact on wet deposition estimates, which is in agreement with other regional model simulations (Bash, 2010; Lin et al., 2007). Measurements in addition to wet deposition will be necessary in evaluating modeled gaseous air-surface exchange parameterizations. Speciated ambient observations provide more insight into the air-surface exchange and atmospheric chemical processes and more observations will further constrain model parameterizations. However, the identification and measurements of the chemical forms of Hg(II) and measurements of the air-surface exchange of Hg(0), Hg(II), and Hg(p) are needed for more direct and robust analyses of the mercury chemical mechanism and dry deposition in photochemical air-quality models.

Disclaimer

Although this work was reviewed by EPA and approved for publication, it may not necessarily reflect official Agency policy.

Acknowledgements

The authors would like to recognize the contribution of Prakash Karamchandani, David Gay, Allan Beidler, Chris Allen, James Beidler, Rich Mason, Madeleine Strum, Marc Houyoux, Ann Marie Carlton, Wyat Appel, Heather Simon, James Kelly, and Carey Jang.

5. REFERNCES

Ariya, P.A., Khalizov, A., Gidas, A., 2002. Reactions of gaseous mercury with atomic and molecular halogens: Kinetics, product studies, and atmospheric implications. Journal of Physical Chemistry A 106, 7310-7320.

Baker, K., Scheff, P., 2007. Photochemical model performance for PM2.5 sulfate, nitrate, ammonium, and precursor species SO2, HNO3, and NH3 at background monitor locations in the central and eastern United States. Atmospheric Environment 41, 6185-6195.

Baker, K., Scheff, P., 2008. Assessing meteorological variable and process relationships to modeled PM2.5 ammonium nitrate and ammonium sulfate in the central United States. Journal of Applied Meteorology and Climatology 47, 2395-2404.

Bash, J.O., 2010. Description and initial simulation of a dynamic bidirectional air-surface exchange model for mercury in Community Multiscale Air Quality (CMAQ) model. Journal of Geophysical Research-Atmospheres 115.

Bullock, O.R., Atkinson, D., Braverman, T., Civerolo, K., Dastoor, A., Davignon, D., Ku, J.Y., Lohman, K., Myers, T.C., Park, R.J., Seigneur, C., Selin, N.E., Sistla, G., Vijayaraghavan, K., 2009. An analysis of simulated wet deposition of mercury from the North American Mercury Model Intercomparison Study. Journal of Geophysical Research-Atmospheres 114.

Bullock, O.R., Brehme, K.A., 2002. Atmospheric mercury simulation using the CMAQ model: formulation description and analysis of wet deposition results. Atmospheric Environment 36, 2135-2146.

Byun, D., Schere, K.L., 2006. Review of the governing equations, computational algorithms, and other components of the models-3 Community Multiscale Air Quality (CMAQ) modeling system. Applied Mechanics Reviews 59, 51-77.

Carlton, A.G., Bhave, P.V., Napelenok, S.L., Edney, E.D., Sarwar, G., Pinder, R.W., Pouliot, G.A., Houyoux, M., 2010. Model Representation of Secondary Organic Aerosol in CMAQv4.7. Environmental Science & Technology 44, 8553-8560.

Carlton, A.G., Turpin, B.J., Altieri, K.E., Seitzinger, S.P., Mathur, R., Roselle, S.J., Weber, R.J., 2008. CMAQ Model Performance Enhanced When In-Cloud Secondary Organic Aerosol is Included: Comparisons of Organic Carbon Predictions with Measurements. Environmental Science & Technology 42, 8798-8802.

Chang, J.S., Brost, R.A., Isaksen, I.S.A., Madronich, S., Middleton, P., Stockwell, W.R., Walcek, C.J., 1987. A 3-Dimensional Eulerian Acid Deposition Model - Physical Concepts and Formulation. J. Geophys. Res.-Atmos. 92, 14681-14700.

Choi, A.L., Pal, W.H., Budtz-Jorgensen, E., Jorgensen, P.J., Salonen, J.T., Tuomainen, T.P., Murata, K., Nielsen, H.P., Petersen, M.S., Askham, J., Grandjean, P., 2009. Methylmercury

Exposure and Adverse Cardiovascular Effects in Faroese Whaling Men. Environmental Health Perspectives 117, 367-372.
Clever, H.L., Johnson, S.A., Derrick, M.E., 1985. The solubility of mercury and some sparing soluble mercury salts in water and aqueous-electrolyte solutions. Journal of Physical and Chemical Reference Data 14, 631-681.
Donohoue, D.L., Bauer, D., Hynes, A.J., 2005. Temperature and pressure dependent rate coefficients for the reaction of Hg with Cl and the reaction of Cl with Cl: A pulsed laser photolysis-pulsed laser induced fluorescence study. Journal of Physical Chemistry A 109, 7732-7741.
Dudhia, J., 1989. Numerical study of convection observed during the winter monsoon experiment using a mesoscale two-dimensional model. Journal of the Atmospheric Sciences 46, 3077-3107.
ENVIRON, 2010. User's Guide Comprehensive Air Quality Model with Extensions version 5.30, www.camx.com. ENVIRON International Corporation, Novato.
Foley, K.M., Roselle, S.J., Appel, K.W., Bhave, P.V., Pleim, J.E., Otte, T.L., Mathur, R., Sarwar, G., Young, J.O., Gilliam, R.C., Nolte, C.G., Kelly, J.T., Gilliland, A.B., Bash, J.O., 2010. Incremental testing of the Community Multiscale Air Quality (CMAQ) modeling system version 4.7. Geoscientific Model Development 3, 205-226.
Gardfeldt, K., Jonsson, M., 2003. Is bimolecular reduction of Hg(II) complexes possible in aqueous systems of environmental importance. Journal of Physical Chemistry A 107, 4478-4482.
Grell, G., Dudhia, J., Stauffer, D., 1994. A description of the fifth-generation Penn State/NCAR mesoscale model (MM5). Technical Note NCAR/TN-398+STR, National Center for Atmosperhic Research, Bouler, CO.
Gustin, M.S., Lindberg, S.E., Weisberg, P.J., 2008. An update on the natural sources and sinks of atmospheric mercury. Appl. Geochem. 23, 482-493.
Hall, B., 1995. The gas-hase oxidation of elemental mercury by ozone. Water Air and Soil Pollution 80, 301-315.
Hammerschmidt, C.R., Fitzgerald, W.F., 2006. Methylmercury in freshwater fish linked to atmospheric mercury deposition. Environmental Science & Technology 40, 7764-7770.
Holmes, C.D., Jacob, D.J., Corbitt, E.S., Mao, J., Yang, X., Talbot, R., Slemr, F., 2010. Global atmospheric model for mercury including oxidation by bromine atoms. Atmospheric Chemistry and Physics 10, 12037-12057.
Houyoux, M.R., Vukovich, J.M., Coats, C.J., Wheeler, N.J.M., Kasibhatla, P.S., 2000. Emission inventory development and processing for the Seasonal Model for Regional Air Quality (SMRAQ) project. Journal of Geophysical Research-Atmospheres 105, 9079-9090.
Kain, J.S., 2004. The Kain-Fritsch convective parameterization: An update. Journal of Applied Meteorology 43, 170-181.
Landis, M.S., Keeler, G.J., 2002. Atmospheric mercury deposition to Lake Michigan during the Lake Michigan Mass Balance Study. Environmental Science & Technology 36, 4518-4524.
Landis, M.S., Stevens, R.K., Schaedlich, F., Prestbo, E.M., 2002. Development and characterization of an annular denuder methodology for the measurement of divalent inorganic reactive gaseous mercury in ambient air. Environmental Science & Technology 36, 3000-3009.
Lin, C.J., Pehkonen, S.O., 1997. Aqueous free radical chemistry of mercury in the presence of iron oxides and ambient aerosol. Atmospheric Environment 31, 4125-4137.

Lin, C.J., Pehkonen, S.O., 1998. Oxidation of elemental mercury by aqueous chlorine (HOCl/OCl-): Implications for tropospheric mercury chemistry. Journal of Geophysical Research-Atmospheres 103, 28093-28102.
Lin, C.J., Pongprueks, P., Rusell Bulock, O., Lindberg, S.E., Pehkonen, S.O., Jang, C., Braverman, T., Ho, T.C., 2007. Scientific uncertainties in atmospheric mercury models II: Sensitivity analysis in the CONUS domain. Atmospheric Environment 41, 6544-6560.
Lindberg, S., Bullock, R., Ebinghaus, R., Engstrom, D., Feng, X.B., Fitzgerald, W., Pirrone, N., Prestbo, E., Seigneur, C., 2007. A synthesis of progress and uncertainties in attributing the sources of mercury in deposition. Ambio 36, 19-32.
Lyman, S.N., Jaffe, D.A., Gustin, M.S., 2010. Release of mercury halides from KCl denuders in the presence of ozone. Atmospheric Chemistry and Physics 10, 8197-8204.
Marsik, F.J., Keeler, G.J., Landis, M.S., 2007. The dry-deposition of speciated mercury to the Florida Everglades: Measurements and modeling. Atmospheric Environment 41, 136-149.
Massman, W.J., 1999. Molecular diffusivities of Hg vapor in air, O-2 and N-2 near STP and the kinematic viscosity and thermal diffusivity of air near STP. Atmospheric Environment 33, 453-457.
Mlawer, E.J., Taubman, S.J., Brown, P.D., Iacono, M.J., Clough, S.A., 1997. Radiative transfer for inhomogeneous atmospheres: RRTM, a validated correlated-k model for the longwave. Journal of Geophysical Research-Atmospheres 102, 16663-16682.
Munthe, J., 1992. THE AQUEOUS OXIDATION OF ELEMENTAL MERCURY BY OZONE. Atmospheric Environment Part a-General Topics 26, 1461-1468.
Nenes, A., Pandis, S.N., Pilinis, C., 1999. Continued development and testing of a new thermodynamic aerosol module for urban and regional air quality models. Atmospheric Environment 33, 1553-1560.
Nobel, C.E., McDonald-Buller, E.C., Kimura, Y., Allen, D.T., 2001. Accounting for spatial variation of ozone productivity in NOx emission trading. Environmental Science & Technology 35, 4397-4407.
Pal, B., Ariya, P.A., 2004a. Gas-phase HO center dot-Initiated reactions of elemental mercury: Kinetics, product studies, and atmospheric implications. Environmental Science & Technology 38, 5555-5566.
Pal, B., Ariya, P.A., 2004b. Studies of ozone initiated reactions of gaseous mercury: kinetics, product studies, and atmospheric implications. Physical Chemistry Chemical Physics 6, 572-579.
Pleim, J.E., Byun, D.W., 2004. Application of a new land-surface, dry deposition, and PBL model in the models-3 Community Multiscale Air Quality (CMAQ) model system. Kluwer Academic Publishers.
Pleim, J.E., Xiu, A., 1995. Development and testing of a surface flux and planetarry boundary-layer model for application in mesoscale models. Journal of Applied Meteorology 34, 16-32.
Pongprueksa, P., Lin, C.J., Lindberg, S.E., Jang, C., Braverman, T., Bullock, O.R., Ho, T.C., Chu, H.W., 2008. Scientific uncertainties in atmospheric mercury models III: Boundary and initial conditions, model grid resolution, and Hg(II) reduction mechanism. Atmospheric Environment 42, 1828-1845.
Reisner, J., Rasmussen, R.M., Bruintjes, R.T., 1998. Explicit forecasting of supercooled liquid water in winter storms using the MM5 mesoscale model. Quarterly Journal of the Royal Meteorological Society 124, 1071-1107.
Russell, A.G., 2008. EPA Supersites Program-related emissions-based particulate matter modeling: Initial applications and advances. J. Air Waste Manage. Assoc. 58, 289-302.

Scheulhammer, A.M., Meyer, M.W., Sandheinrich, M.B., Murray, M.W., 2007. Effects of environmental methylmercury on the health of wild birds, mammals, and fish. Ambio 36, 12-18.

Schroeder, W.H., Munthe, J., 1998. Atmospheric mercury - An overview. Atmospheric Environment 32, 809-822.

Seigneur, C., Abeck, H., Chia, G., Reinhard, M., Bloom, N.S., Prestbo, E., Saxena, P., 1998. Mercury adsorption to elemental carbon (soot) particles and atmospheric particulate matter. Atmospheric Environment 32, 2649-2657.

Selin, N.E., 2009. Global Biogeochemical Cycling of Mercury: A Review. Annual Review of Environment and Resources 34, 43-63.

Selin, N.E., Jacob, D.J., Park, R.J., Yantosca, R.M., Strode, S., Jaegle, L., Jaffe, D., 2007. Chemical cycling and deposition of atmospheric mercury: Global constraints from observations. Journal of Geophysical Research-Atmospheres 112.

Selin, N.E., Sunderland, E.M., Knightes, C.D., Mason, R.A., 2010. Sources of Mercury Exposure for US Seafood Consumers: Implications for Policy. Environmental Health Perspectives 118, 137-143.

Si, L., Ariya, P.A., 2008. Reduction of oxidized mercury species by dicarboxylic acids (C-2-C-4): Kinetic and product studies. Environmental Science & Technology 42, 5150-5155.

Sommar, J., Gardfeldt, K., Stromberg, D., Feng, X.B., 2001. A kinetic study of the gas-phase reaction between the hydroxyl radical and atomic mercury. Atmospheric Environment 35, 3049-3054.

Strader, R., Lurmann, F., Pandis, S.N., 1999. Evaluation of secondary organic aerosol formation in winter. Atmospheric Environment 33, 4849-4863.

Tokos, J.J.S., Hall, B., Calhoun, J.A., Prestbo, E.M., 1998. Homogeneous gas-phase reaction of Hg-0 with H2O2, O-3, CH3I, and (CH3)(2)S: Implications for atmospheric Hg cycling. Atmospheric Environment 32, 823-827.

U.S. Environmental Protection Agency, 2007. Clean Air Mercury Rule (CAMR), Vol. 72, No. 202, ed. Federal Register.

U.S. Environmental Protection Agency, 2010. National Emissions Standards for Hazardous Air Pollutants from the Portland Cement Manufacturing Industry and Standards of Performance for Portland Cement Plants, Vol. 75, No. 174, ed. Federal Register.

U.S. Environmental Protection Agency, 2011. National Emissions Standards for Hazardous Air Pollutants for Major Sources: Industrial, Commercial, and Institutional Boilers and Process Heaters; Final Rule, Vol. 76, No. 54, ed. Federal Register.

Van Loon, L., Mader, E., Scott, S.L., 2000. Reduction of the aqueous mercuric ion by sulfite: UV spectrum of HgSO3 and its intramolecular redox reaction. Journal of Physical Chemistry A 104, 1621-1626.

Van Loon, L.L., Mader, E.A., Scott, S.L., 2001. Sulfite stabilization and reduction of the aqueous mercuric ion: Kinetic determination of sequential formation constants. Journal of Physical Chemistry A 105, 3190-3195.

Vermette, S., Lindberg, S., Bloom, N., 1995. Field-tests for a regional mercury deposition network - sampling design and preliminary test-results. Atmospheric Environment 29, 1247-1251.

Vijayaraghavan, K., Seigneur, C., Karamchandani, P., Chen, S.Y., 2007. Development and application of a multipollutant model for atmospheric mercury deposition. Journal of Applied Meteorology and Climatology 46, 1341-1353.

Wagstrom, K.M., Pandis, S.N., Yarwood, G., Wilson, G.M., Morris, R.E., 2008. Development and application of a computationally efficient particulate matter apportionment algorithm in a three-dimensional chemical transport model. Atmospheric Environment 42, 5650-5659.

Wesely, M.L., 1989. Parameterization of surface resistances to gaseous dry deposition in regional-scale numerical-moels. Atmospheric Environment 23, 1293-1304.

Wisconsin Department of Natural Resources, 2008. Publication AM-383-2007 - Preliminary Mercury Finding Pursuant to Section 285.27(2)(b), Wisconsin Statutes.

Xiao, Z.F., Stromberg, D., Lindqvist, O., 1995. INFLUENCE OF HUMIC SUBSTANCES ON PHOTOLYSIS OF DIVALENT MERCURY IN AQUEOUS-SOLUTION. Water Air and Soil Pollution 80, 789-798.

Yarwood, G., Rao, S., Tocke, M., Whitten, G.Z., 2005. Updates to the carbon bond mechanism: CB05. Report to the U.S. Environmental Protection Agency. http://www.camx.com/publ/pdfs/CB05_Final_Report_120805.pdf. ENVIRON International Corporation, Novato.

Zhang, L.M., Wright, L.P., Blanchard, P., 2009. A review of current knowledge concerning dry deposition of atmospheric mercury. Atmospheric Environment 43, 5853-5864.

List of Tables

References from Tables

(Ariya et al., 2002; Donohoue et al., 2005; Hall, 1995; Lin and Pehkonen, 1997, 1998; Munthe, 1992; Pal and Ariya, 2004a; Seigneur et al., 1998; Si and Ariya, 2008; Sommar et al., 2001; Tokos et al., 1998; Van Loon et al., 2000; Van Loon et al., 2001; Xiao et al., 1995) (Pal and Ariya, 2004b)

Sillen, G.L. and A.E. Martell, (Eds.). 1964. Stability constants of metal ion complexes, Spec. Publ. Chem. Soc., 17, 754.

List of Figures

664

Table 1. Mercury oxidation and reduction reactions and reaction rates in CMAQ 4.7.1 and CAMx 5.30.

Table 2. Annual total emissions (Mg) for 2005 in the 36 km modeling domain.

	Annual Emissions (Mg/year)				Speciation Percentage (%)		
Sector	Hg(0)	Hg(II)	Hg(p)	Total	Hg(0)	Hg(II)	Hg(p)
Mobile	0.7	0.3	0.1	1.1	65	24	11
Non-Point/Area	2.8	1.0	0.6	4.4	64	22	14
Point: EGU	27.4	19.1	1.5	48.0	57	40	3
Point: non-EGU	26.8	9.5	5.6	41.9	64	23	13
Canada/Mexico (within model domain)	4.1	2.6	0.8	7.5	55	35	10
Land - Direct	11.0	0.0	0.0	11.0	100	0	0
Land Re-emission	143.3	0.0	0.0	143.3	100	0	0
Ocean - Direct	6.6	0.0	0.0	6.6	100	0	0
Ocean Re-emission	51.3	0.0	0.0	51.3	100	0	0
Volcanic	3.7	0.0	0.0	3.7	100	0	0
Total	277.7	32.5	8.5	318.7	87	10	3

Table 3. Annual total modeled mercury deposition (Mg) in the 36 km modeling domain.

		CAMx		CAMx SENS		CMAQ		CMAQ BIDI	
	Specie	**Sum[a]**	**%[b]**	**Sum[a]**	**%[b]**	**Sum[a]**	**%[b]**	**Sum[a]**	**%[b]**
Dry Deposition	Hg(0)	0	0	157	32	138	26	-6	-1
	Hg(II)	259	79	269	54	171	32	171	43
	Hg(p)	0	0	0	0	1	0	1	0
Wet Deposition	Hg(0)	0	0	0	0	0	0	0	0
	Hg(II)	63	19	64	13	214	39	214	54
	Hg(p)	6	2	6	1	17	3	17	4
Total Deposition	Hg(0)	0	0	157	32	138	26	-5	-1
	Hg(II)	322	98	333	67	385	71	385	97
	Hg(p)	6	2	6	1	19	3	19	5
Total Dry Deposition		259	79	427	86	311	57	167	42
Total Wet Deposition		69	21	70	14	231	43	231	58
Total Deposition		328		497		542		398	

[a]Annual domain sum (Mg)

[b]Percent of total deposition

Table 4. Model performance metrics by season for total mercury wet deposition over the 12 km eastern and 12 km western domains.

				CAMx					CMAQ				
Domain	Season	N	Observed (ng/m^2)	Predicted (ng/m^2)	Bias (ng/m^2)	Error (ng/m^2)	Fractional Bias (%)	Fractional Error (%)	Predicted (ng/m^2)	Bias (ng/m^2)	Error (ng/m^2)	Fractional Bias (%)	Fractional Error (%)
eastern U.S.	Jan,Feb,Mar	620	167	152	-14	102	-7	69	270	103	158	33	72
eastern U.S.	Apr,May,Jun	670	272	151	-121	175	-42	79	283	10	208	8	75
eastern U.S.	Jul,Aug,Sep	645	348	155	-193	242	-60	91	177	-171	253	-45	91
eastern U.S.	Oct,Nov,Dec	578	144	118	-26	89	-13	71	205	61	121	35	72
western U.S.	Jan,Feb,Mar	82	133	128	-6	90	-18	82	597	464	483	110	121
western U.S.	Apr,May,Jun	90	175	165	-11	118	-28	82	642	467	513	85	109
western U.S.	Jul,Aug,Sep	66	189	159	-30	122	-20	77	399	210	295	51	89
western U.S.	Oct,Nov,Dec	74	133	126	-7	86	-23	78	449	316	341	78	105

Metrics of annual averaged concentrations:
N=88
CAMX FBIAS,FERROR = -41 and 45
CMAQ FBIAS, FERROR = 15 and 33

Figure 1. Model domains and locations of AMNet and MDN monitors.

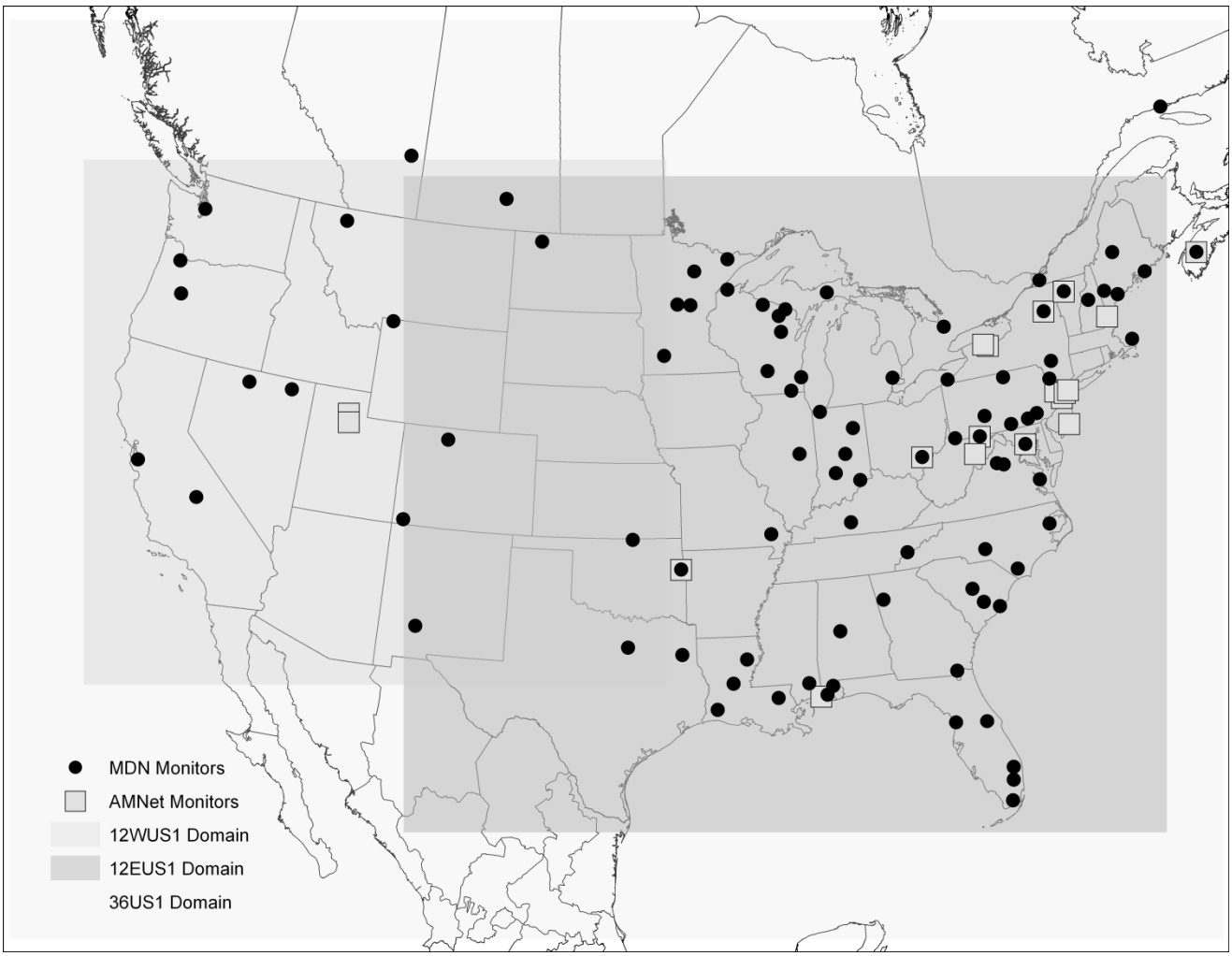

Figure 2. Annual total deposition for base CMAQ (top left), CMAQ-BIDI (top right), base CAMx (bottom left), and CAMx sensitivity (bottom right).

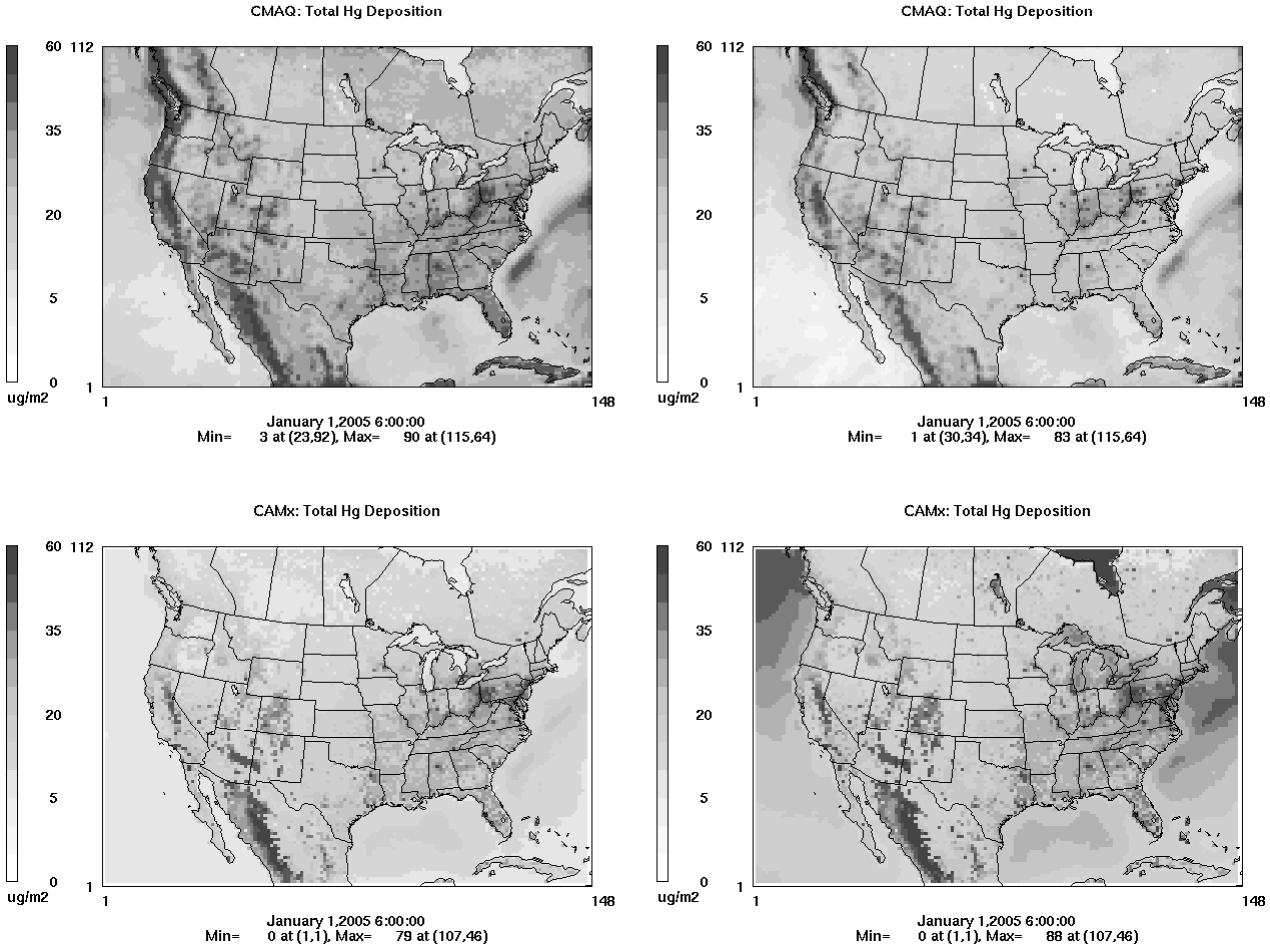

Figure 3. Monthly distributions of observed and modeled weekly rainfall at MDN locations in the eastern 12 km domain (top) and western 12 km domain (bottom).

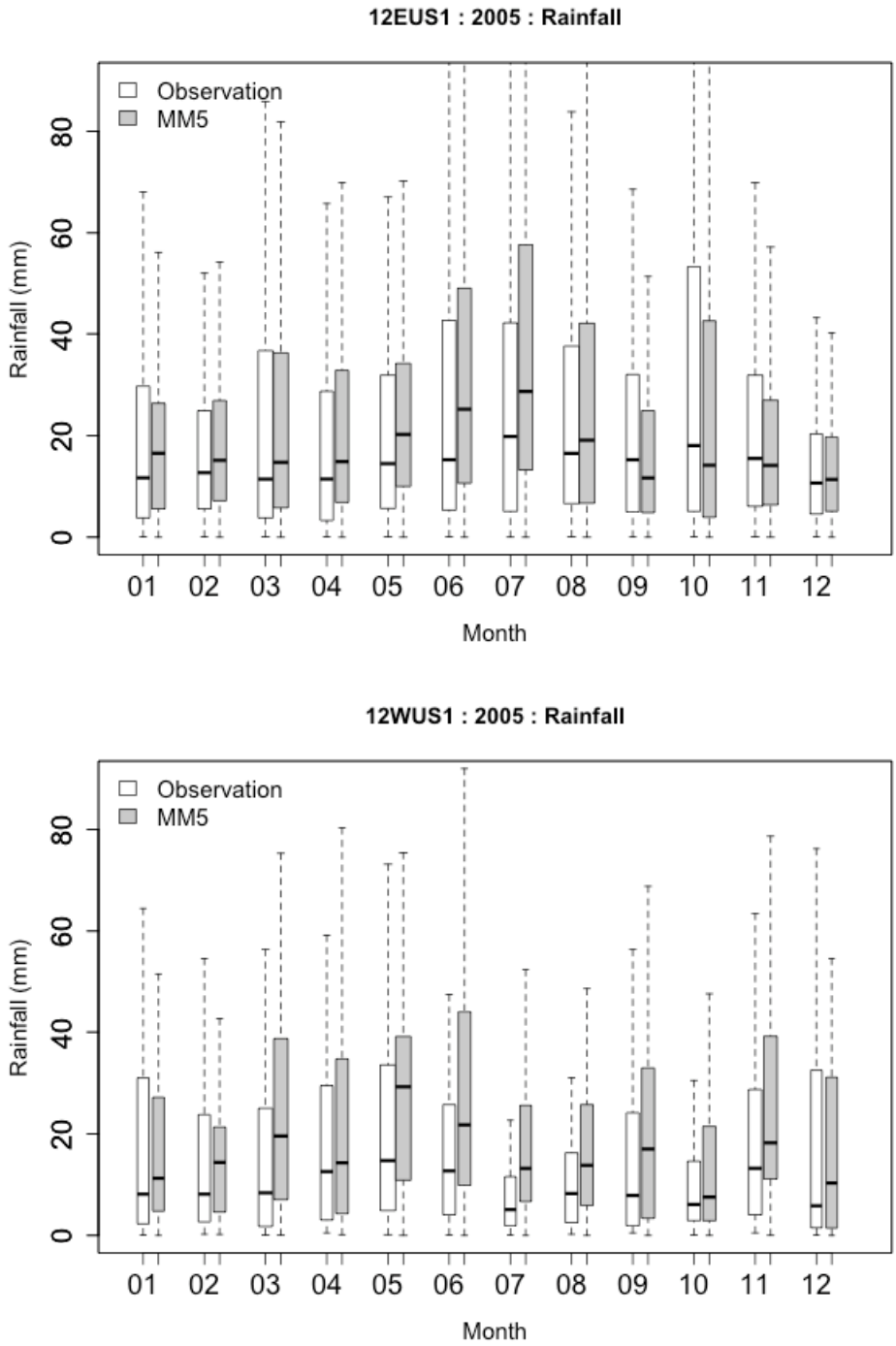

Figure 4. Monthly distributions of observed and modeled weekly total mercury wet deposition at MDN locations in the eastern 12 km domain (top) and western 12 km domain (bottom).

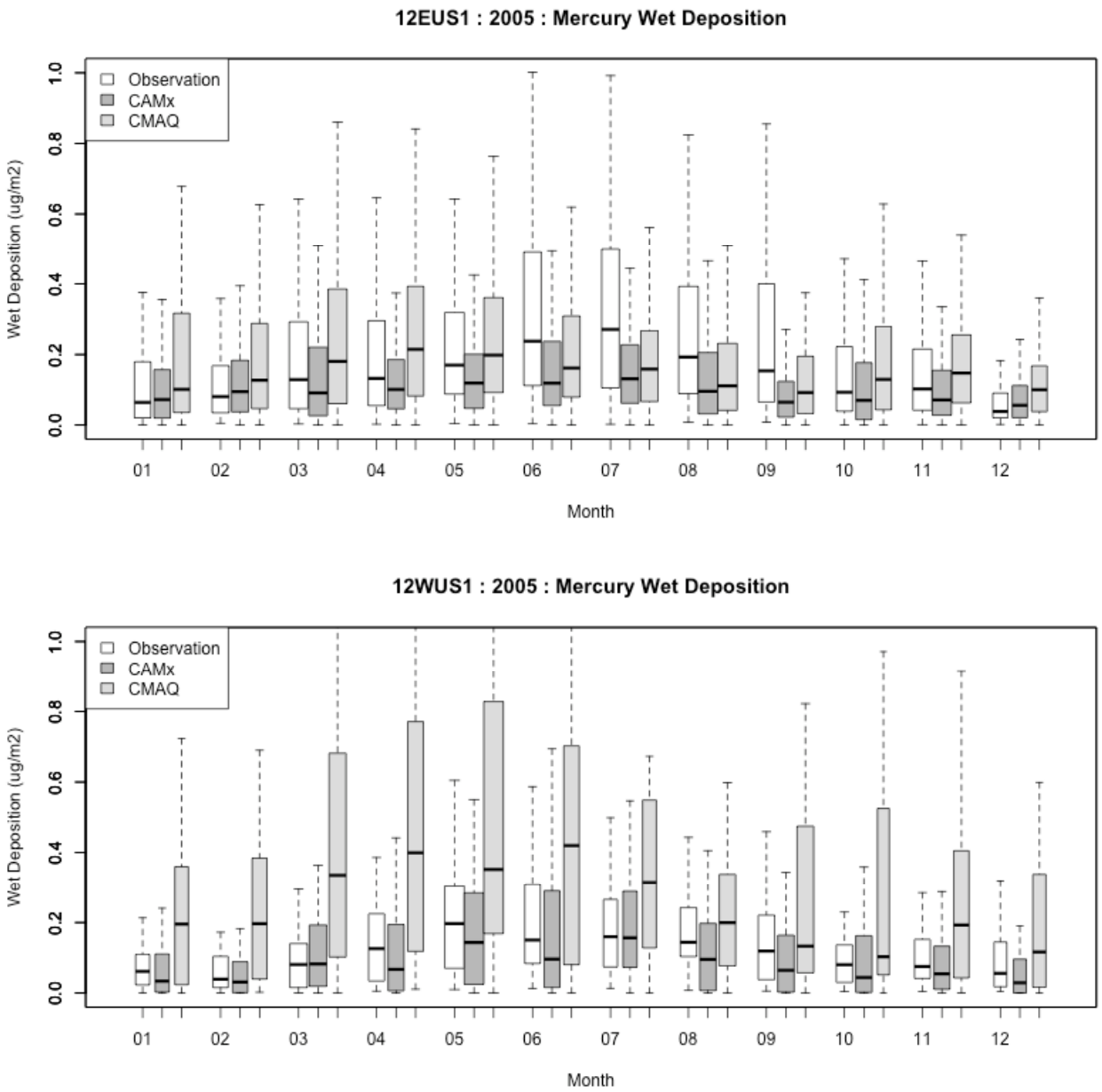

Figure 5. Monthly distributions of 2009 observed and 2005 modeled hourly ambient specied mercury at AMNet locations in the eastern 12 km domain: Hg(0) at top, Hg(II) in middle, and Hg(p) at bottom.

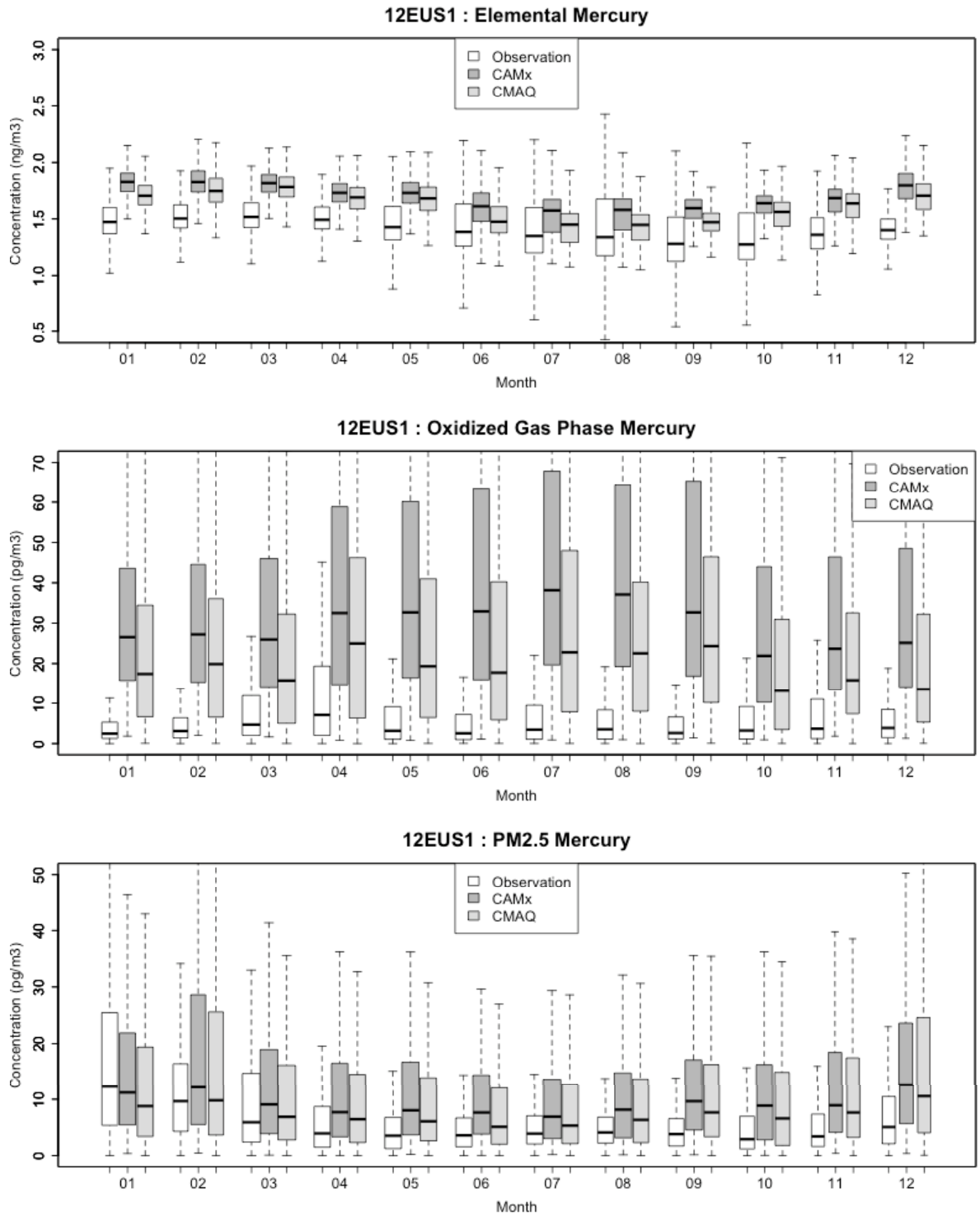

Figure 6. Hourly distributions of 2009 observed and 2005 modeled hourly ambient specied mercury at AMNet locations in the eastern 12 km domain: Hg(0) at top, Hg(II) in middle, and Hg(p) at bottom.

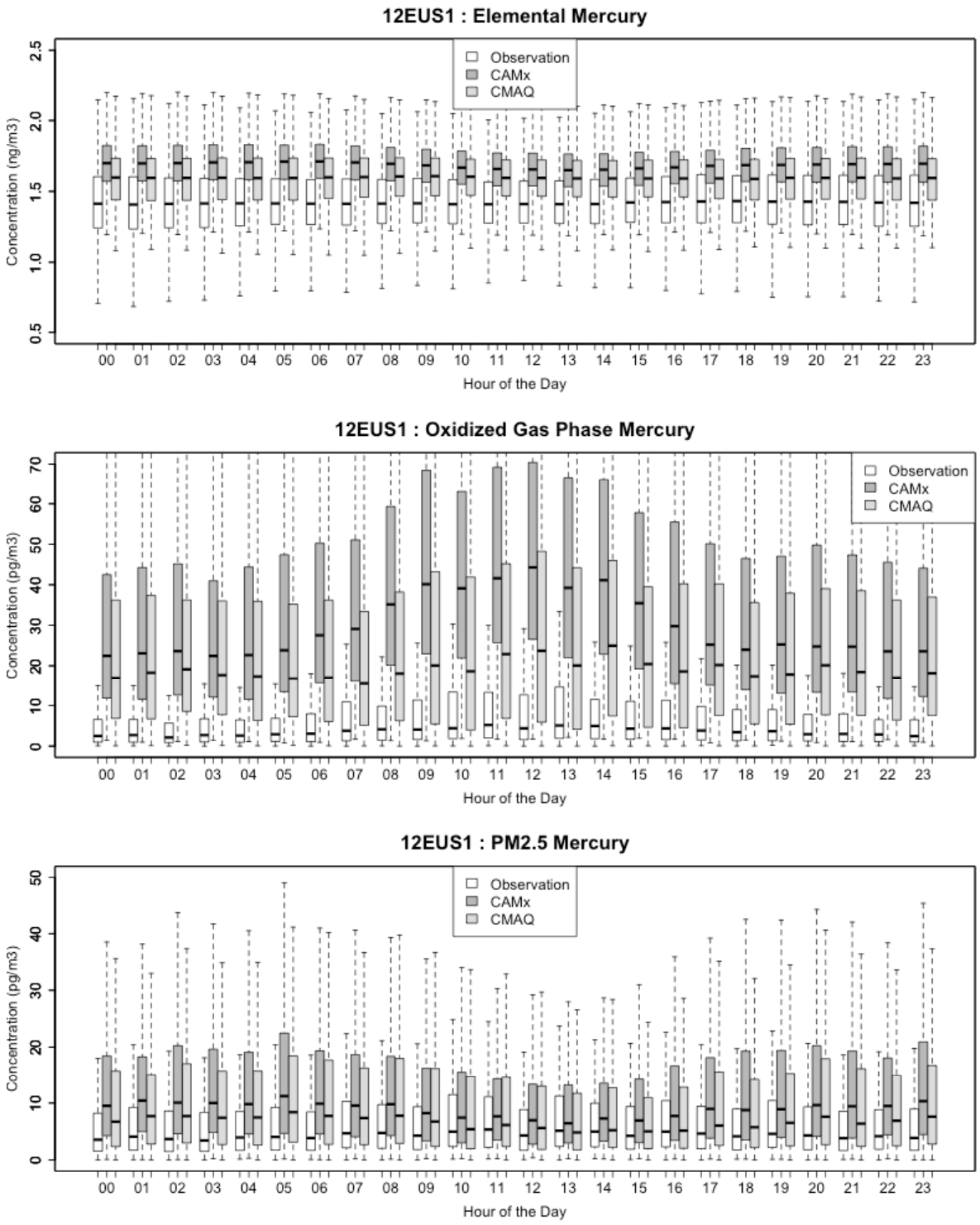

Figure 7. Distribution of observed and modeled total reactive mercury (Hg(II) + Hg(p) by month at top, Hg(p) as a fraction of total reactive mercury by month in middle, and Hg(p) as a fraction of total reactive mercury by hour of the day at bottom.

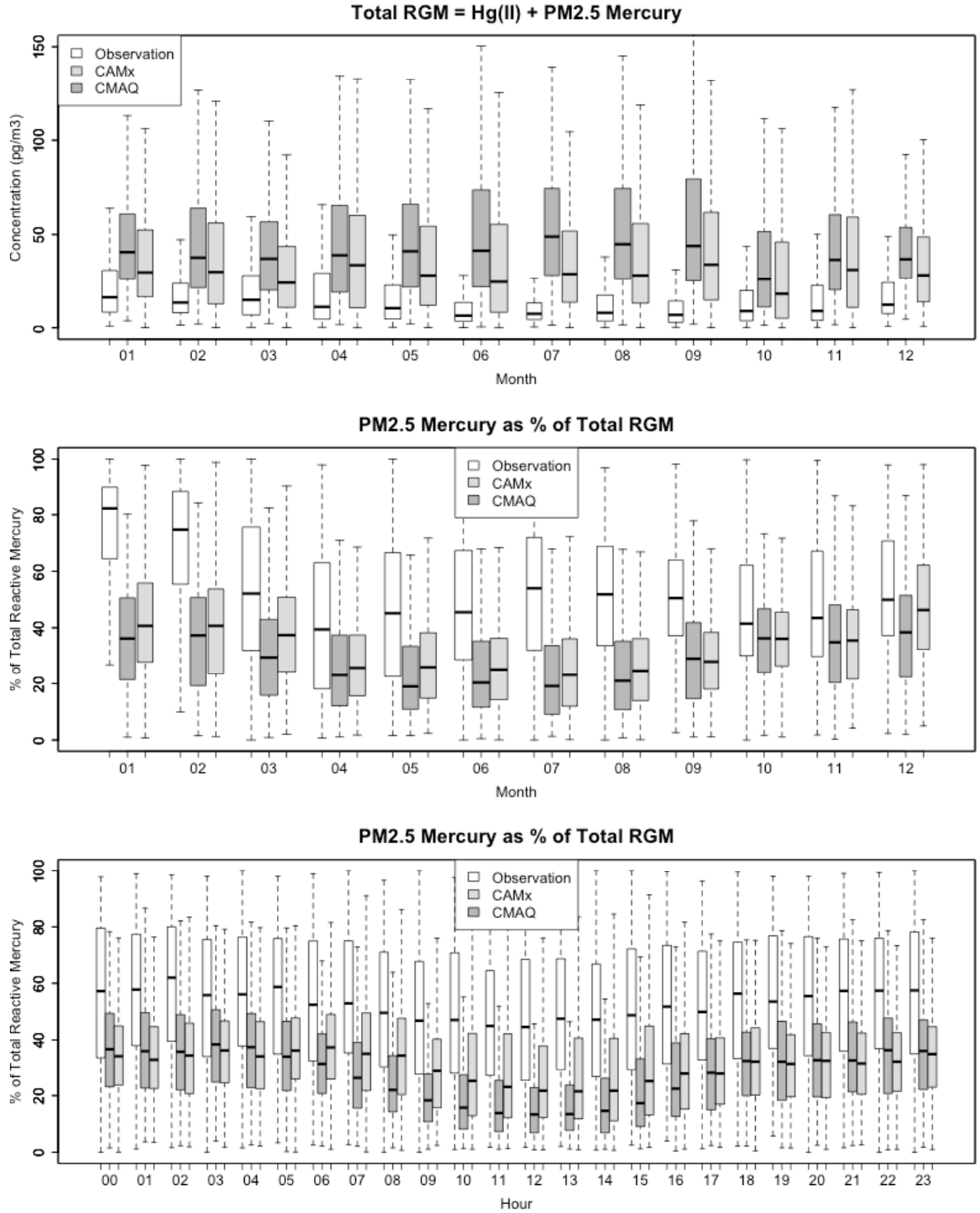

Figure S-1. Annual dry deposition as a fraction of total deposition for base CMAQ (top left), CMAQ-BIDI (top right), base CAMx (bottom left), and CAMx sensitivity (bottom right).

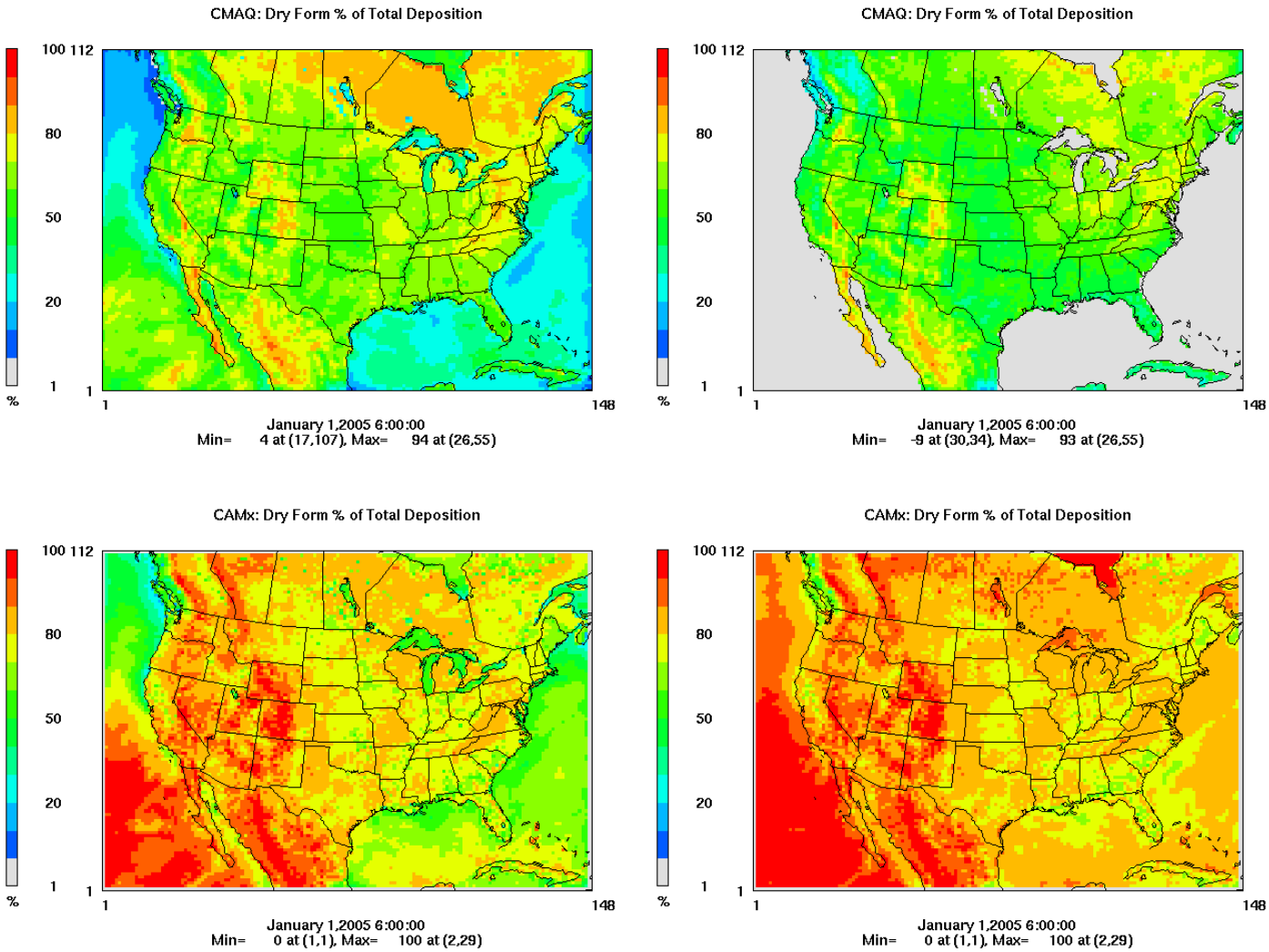

Figure S-2. Modeled contribution (%) to total mercury wet and dry deposition from initial conditions for the first 40 days of winter and summer modeling periods.

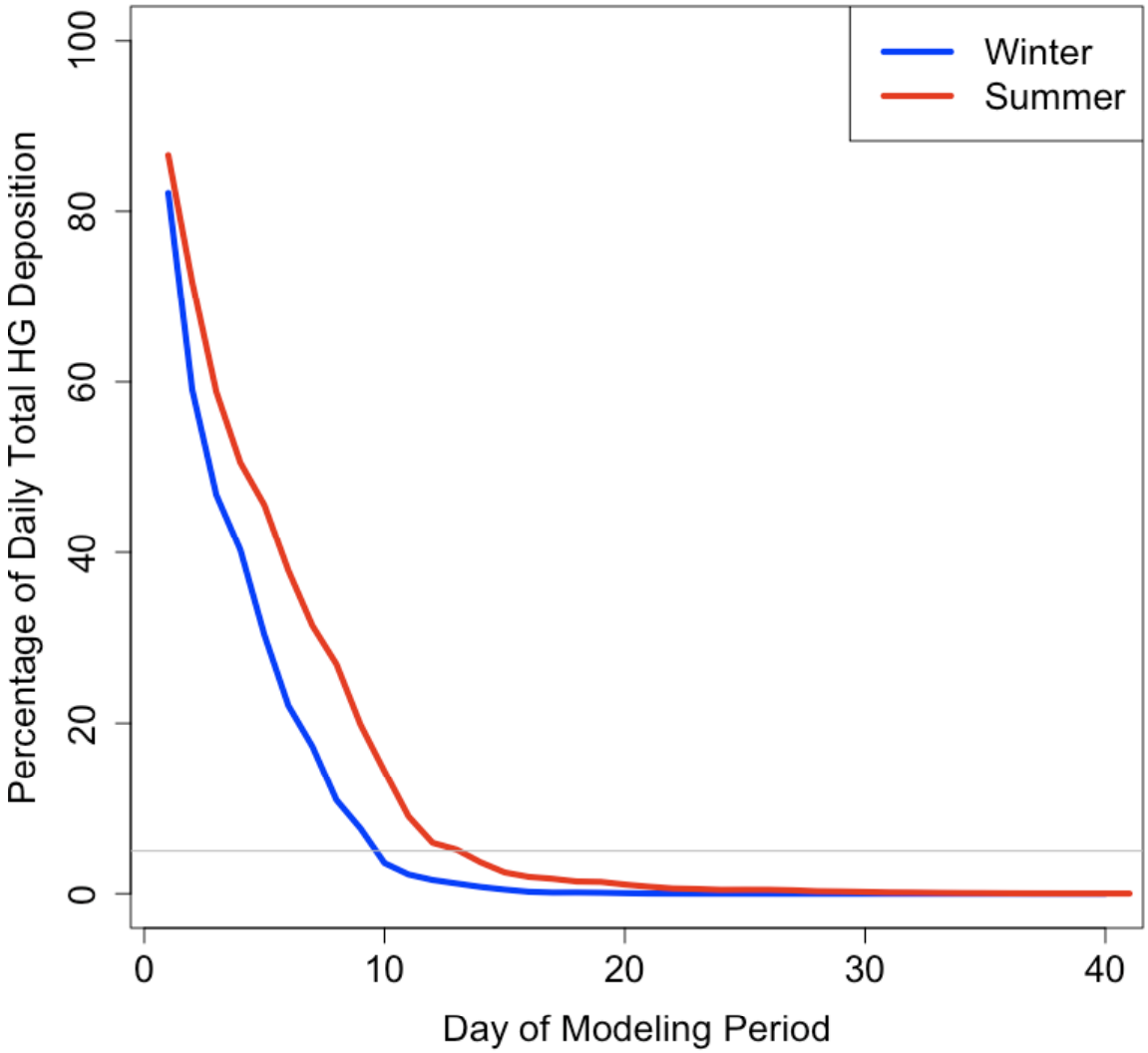

Figure S-3. Warm month (April through August) average difference (modeled-observed) in total mercury wet deposition at each MDN monitor location at 12 km resolution for CMAQ (top) and CAMx (bottom).

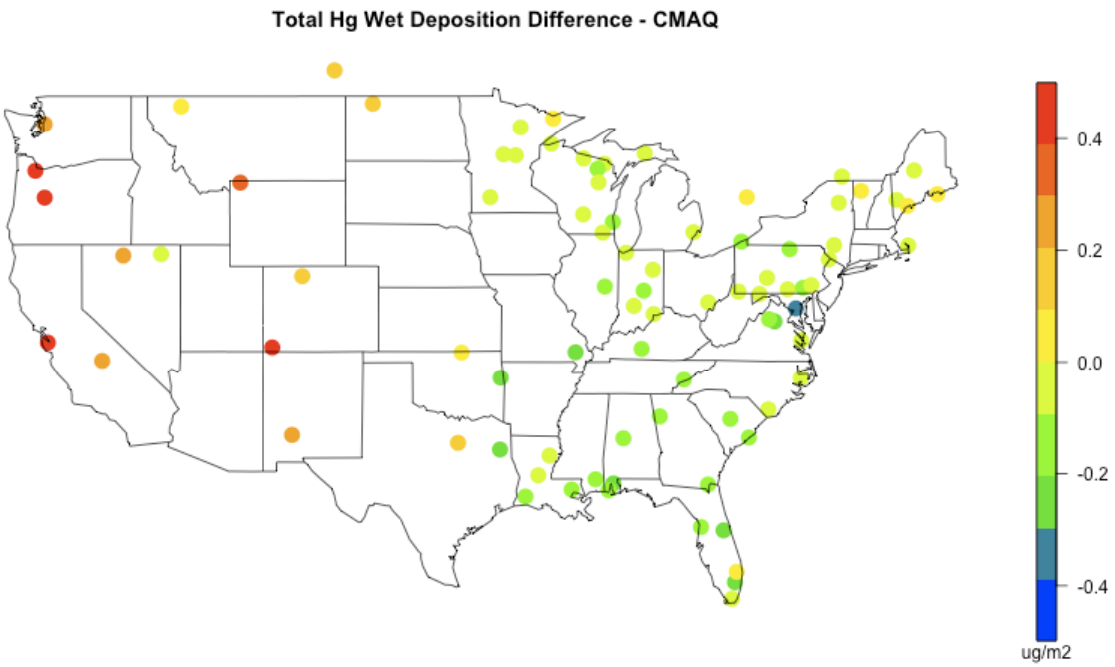

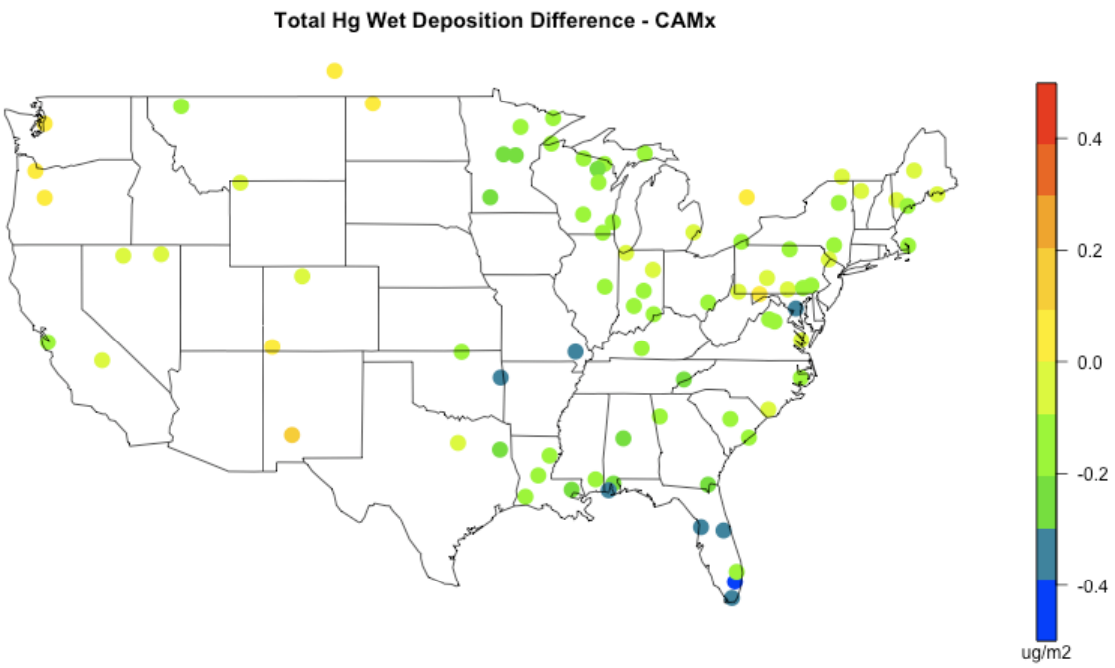

Figure S-4. Monthly distributions of observed and modeled weekly total mercury wet deposition at MDN locations in the eastern (top) and western (bottom) portions of the 36 km model domain. Modeled results include CAMx sensitivity and CMAQ-BIDI.

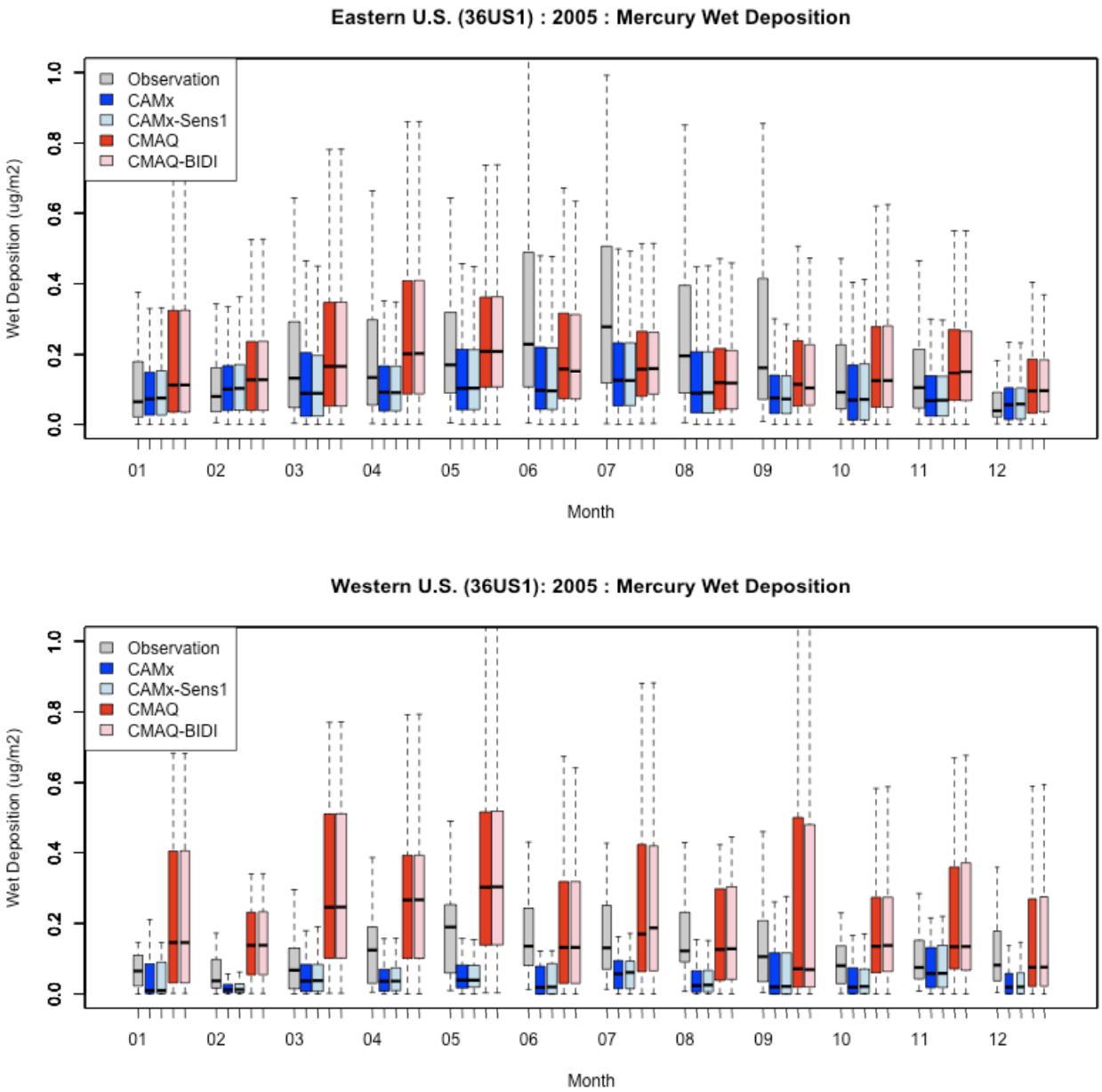

Figure S-5. Annual average rainfall ratio (modeled/observed) compared to annual average total mercury wet deposition ratio (modeled/observed) for CMAQ (top) and CAMx (bottom).

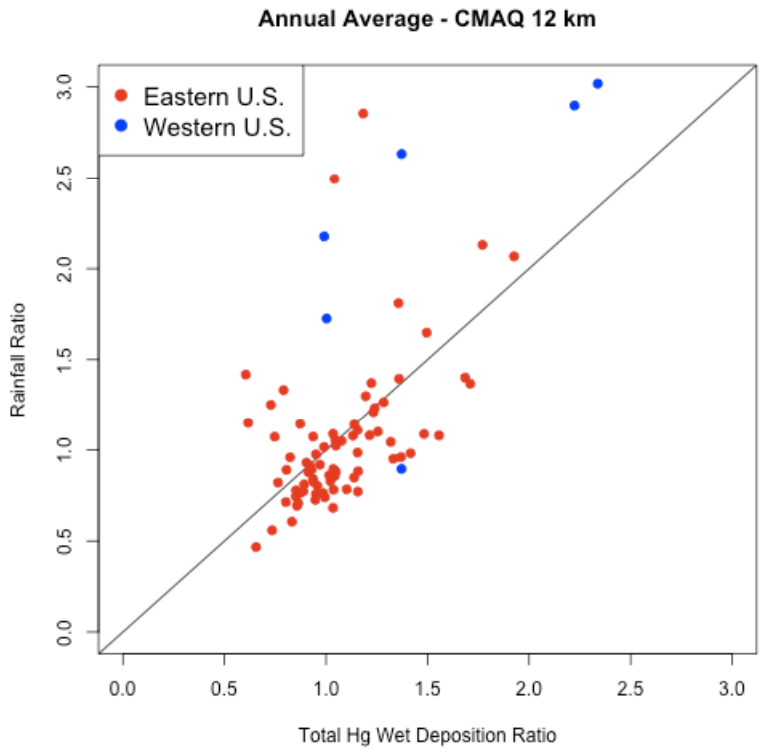

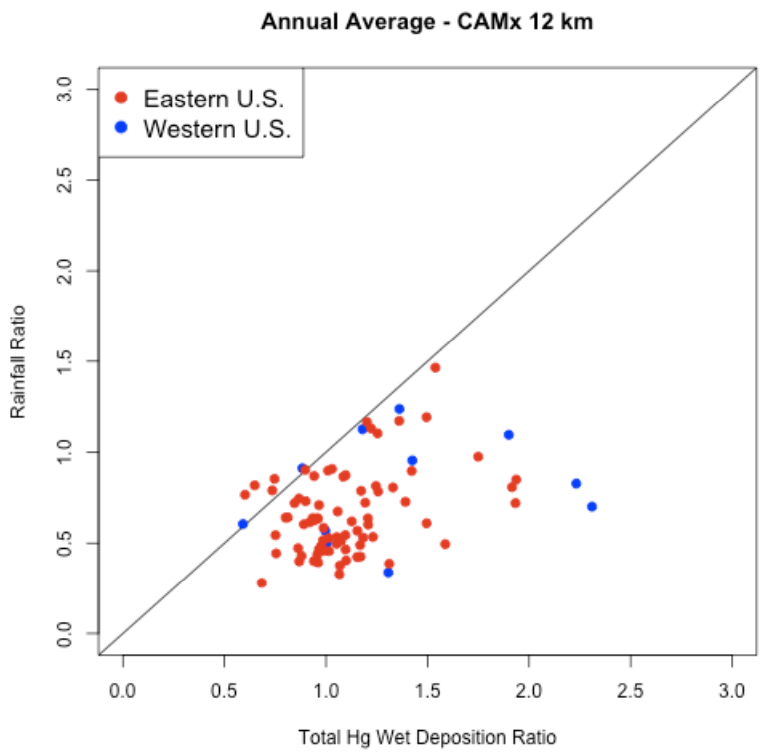

Figure S-6. Monthly distributions of 2009 observed and 2005 modeled hourly ambient specied mercury at AMNet locations in the 36 km domain: Hg(0) at top, Hg(II) in middle, and Hg(p) at bottom. Modeled results include CAMx sensitivity and CMAQ-BIDI.

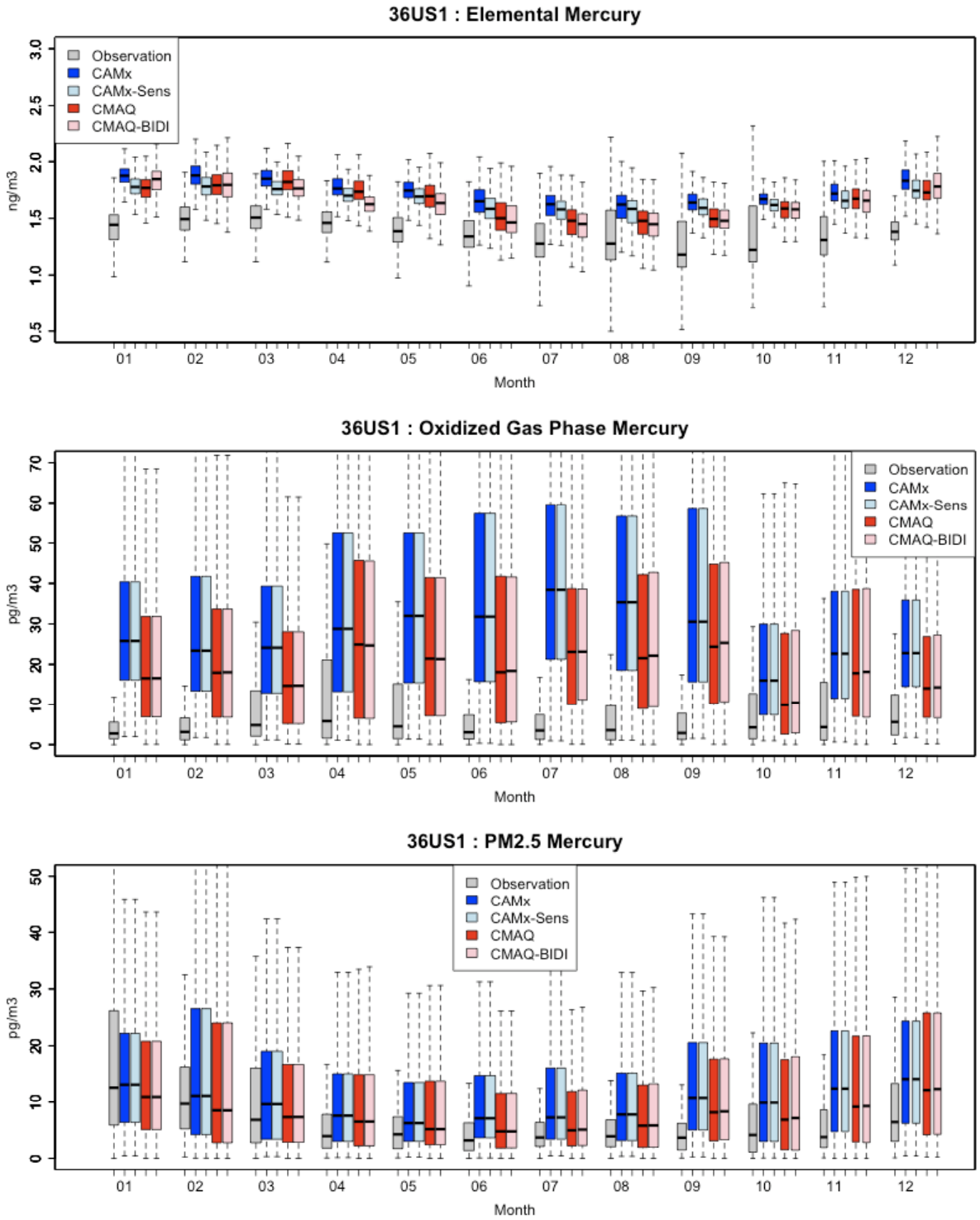

Figure S-7. Distribution of modeled dry deposition velocities for Hg(0) (top) and Hg(II) (bottom) by month of the year at AMnet monitor locations in the 36 km model domain.

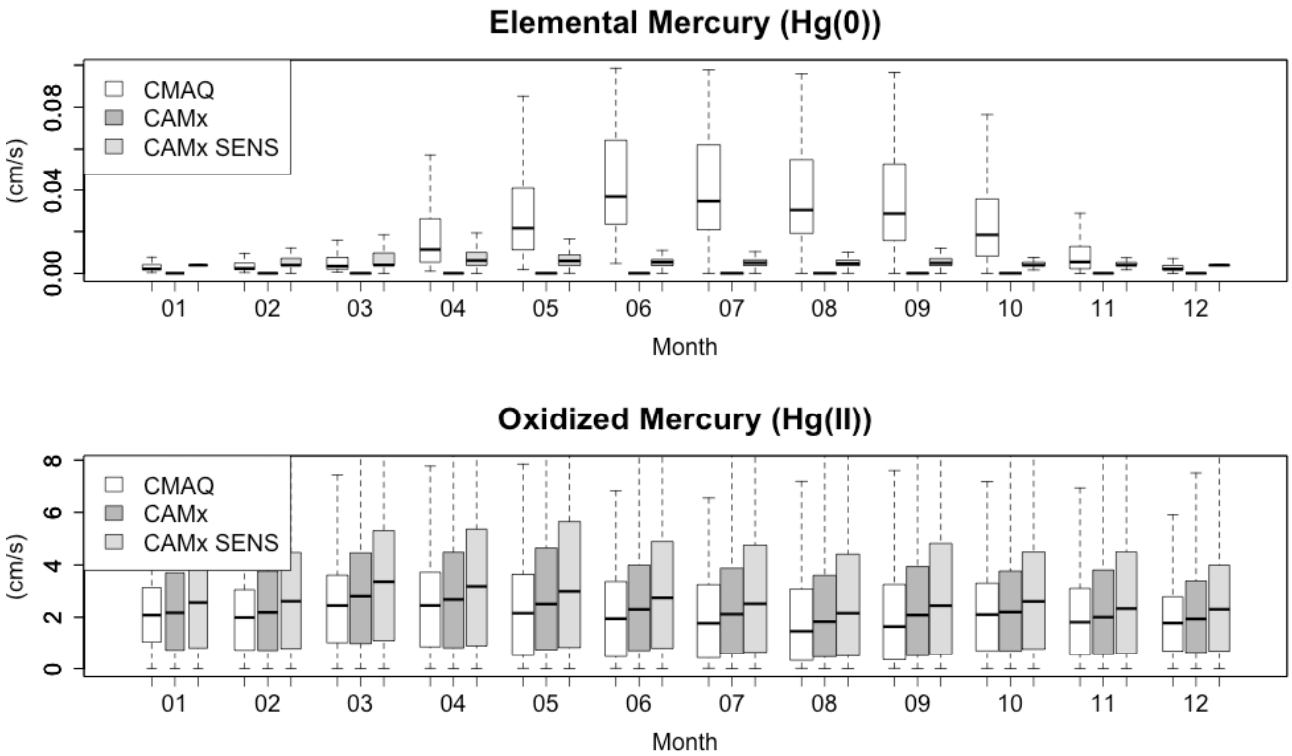

Figure S-8. Distribution of modeled dry deposition velocities for Hg(0) (top) and Hg(II) (bottom) by hour of the day at AMnet monitor locations in the 36 km model domain.